Climate Dynamics (1996) 12:523–533

Climate Dynamics

The effect of reduced ocean overturning on the climate of the last glacial maximum

Richard Bintanja* and Johannes Oerlemans

Institute for Marine and Atmospheric Research Utrecht, Utrecht University, PO Box 80005, 3508 TA Utrecht, The Netherlands

Received: 16 March 1995 / Accepted: 18 December 1995

Abstract. This study focuses on the differences between the present-day climate and the climate of the last glacial maximum (LGM) of 18000 y BP using a zonally averaged energy balance climate model. The ocean is represented by a 2-D model with prescribed overturning pattern in which the overturning velocities can be adjusted freely. We discuss what influence the use of ice-age conditions (i.e. enhanced land-ice cover, reduced CO_2-concentration and reduced oceanic overturning rate) has on the differences between ice-age and present-day climate. When compared to LGM sea-surface temperatures derived from proxy data, the model is able to simulate fairly well the important features of the meridional distribution of these temperature differences. Applying reduced ocean overturning rates during the LGM significantly decreases poleward heat transport in the oceans, thereby allowing for additional cooling of the polar regions and less cooling of the equatorial region. As a result, the agreement with CLIMAP proxy temperature differences increases, especially in the equatorial region. This mechanism can explain the slight differences in the CLIMAP proxy equatorial surface temperatures between the LGM and the present-day climate.

Introduction

Paleoclimatic data indicates that the glacial-interglacial cycle of the Earth's climate system exhibits a dominant period of about 100 ky. It seems to be broadly accepted that quasi-periodic Milankovitch insolation variations are the primary cause for these climatic fluctuations. However, it has been discovered that solar insolation variations alone cannot explain the observed magnitude and time span of climatic variations. Therefore, additional climatic feedback mechanisms are effectively modulating the climate signal. Oerlemans (1980) used an ice-dynamical bedrock-adjustment model and was able to simulate realistic glacial-interglacial periodicity, that is, slow ice sheet build-up and rapid decline. Adding an energy balance climate model (EBCM) to such a model (e.g. Pollard 1982; Peltier and Marshall 1995, and references herein) seems to yield qualitatively similar results. Note, however, that these models require some fine tuning to match the observed ice sheet fluctuations.

Rind et al. (1989) used the GISS GCM to investigate the ability of the model to build up ice sheets at the required locations at about 110 ky BP, the approximate period of initiation of the last ice age. They found that their model was unable to maintain snow cover through the summer, and hence to obtain a positive annual mass balance, even under unrealistically favourable conditions. On the other hand, Oglesby (1990) used the NCAR CCM to investigate its ability to form ice sheets in the Northern Hemisphere and concluded that the model was able to sustain snow cover through summer at locations known as source regions for Pleistocene ice sheets. These inter-model differences demonstrate the lack in our current understanding of the important mechanisms for ice-age initiation.

Another way to gain understanding in the causes of the ice-age cycle is to study the differences between glacial and interglacial climatic conditions. The mechanisms causing these differences are likely to play a role also in the occurrence of the glacial-interglacial cycles, although it must be realized that some of these mechanisms (e.g. CO_2-variations) appear to lag behind global cooling and ice-sheet build-up. In this study, we will attempt to simulate the climate of the Last Glacial Maximum (LGM, hereafter) (18 ky before present), since the differences in LGM and current climate are relatively large and since relatively much is known about the LGM-climate from proxy data.

The climate during the LGM has been simulated in various modelling studies (e.g. Gates 1976; Hansen et

Correspondence to: R. Bintanja

**Present address:* Royal Netherlands Meteorological Institute, PO Box 201, 3730 AE De Bilt, The Netherlands

al. 1984; Manabe and Broccoli 1985a; Kutzbach and Guetter 1986; Rind 1987; Hyde et al. 1989; Harvey 1989a, to name but a few). In these studies, the LGM climate is calculated on the basis of LGM boundary conditions and is compared with climatic conditions as reconstructed from proxy data. This tests the ability of a climate model to satisfactory simulate other than present-day climates, from which the sensitivity of the model to different boundary conditions can be investigated. Such tests, if successful, would significantly increase the value of simulations of future climate.

The majority of these modelling studies of the ice-age climate used atmospheric models with prescribed SST and sea-ice distribution. Only Manabe and Broccoli (1985a) and Hyde et al. (1989) coupled the atmosphere to a mixed layer ocean and calculated the surface temperature explicitly. In most of the studies mentioned perpetual July and/or January climates were simulated. Hyde et al. (1989) used a seasonal 2-D EBCM coupled to a mixed layer ocean. They showed that the LGM temperature field predicted by their EBCM agrees well with results obtained with the NCAR community climate model (Kutzbach and Guetter 1986). This indicates that the differences in the heat budget terms between the LGM and current climate (which can be simulated with sufficient accuracy using an EBCM) are probably more important than the differences in atmospheric dynamics. Further, they showed that the altered energy balance distribution of the earth-atmosphere system is consistent with the SST-estimates from CLIMAP (1976). Therefore, there is probably justification in using an EBCM with simplified dynamics to study differences between the LGM and present-day climate. Harvey (1989a) used an EBCM to study the climate of the LGM and concluded that temporal variations in aerosols and cloud optical properties played an important role in cooling of the climate during the LGM.

In contrast to earlier attempts to simulate the characteristics of the LGM-climate, we will study additionally the effect of different oceanic overturning rates during the LGM. This means that our model allows the ocean-atmosphere system to alter significantly its oceanic poleward heat transport during ice-age conditions. For this purpose, we will use an EBCM resolving the seasonal cycle coupled to a simple ocean model in which overturning is prescribed.

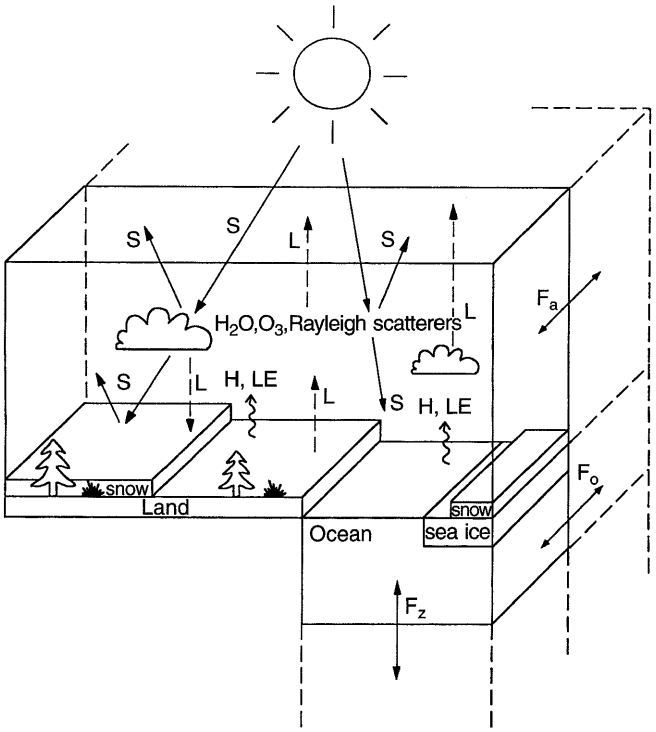

Fig. 1. Schematic illustration of a zonal band from the model, containing land, ocean, partial snow and sea-ice cover. *S* and *L* represent the shortwave and longwave radiative fluxes, respectively. *H* and *LE* are the vertical turbulent fluxes of sensible and latent heat at the surface, respectively. F_a and F_0 represent the total meridional heat fluxes in the atmosphere and ocean, respectively. F_z is the vertical heat flux between the upper ocean layer and the deep ocean

Brief model outline and present-day climate

A complete description of the model used in this study is presented by Bintanja (1995). Since both the atmospheric part (e.g. Harvey 1988a) and oceanic part (e.g. Watts and Morantine 1991) of the model are well-known, only the important features will be summarized here.

The atmospheric part of the model is generally known as an energy balance climate model (EBCM), which consists of a vertically and zonally averaged atmosphere (Fig. 1) with the surface air temperature as the basic prognostic variable. The radiative fluxes at the top of the atmosphere and at the surface are parametrized in terms of the relevant parameters, such as surface air temperature, CO_2-content, cloud amount and cloud optical thickness (Bintanja 1996). At the surface, the land and ocean exchange turbulent energy with the atmosphere. Meridional transport of energy is incorporated as a diffusive process in terms of the surface air temperature with prescribed, latitudinally varying diffusion coefficients. The albedo of land is dependent on (1) the surface type (grass, forest or land ice) and (2) the amount of snow cover. The distribution of surface types is prescribed and held constant throughout the experiments, whereas the amount of snow on land is allowed to vary with the surface air temperature (Robock 1980) without calculating explicitly the moisture budget.

The oceanic part of the model represents a zonal mean overturning ocean (Fig. 2), in which upwelling takes place in the entire basin except in two downwelling regions near both poles. No flow of water across the equator takes place. The mean upwelling velocity in the current climatic state is 4 m yr^{-1} (Hoffert et al. 1980), which in our model outline implies overturning rates of 17.2 and 20.2 Sv in the Northern (NH) and the Southern Hemisphere (SH), respectively. These overturning rates are in reasonable agreement with ob-

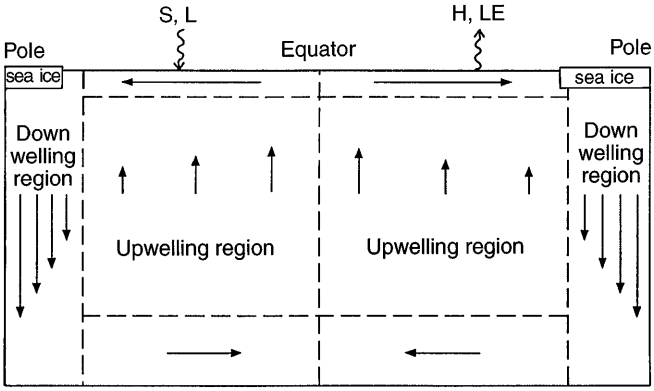

Fig. 2. Schematic illustration of the zonal mean thermohaline circulation in the ocean. The arrows indicate the direction of the flow. S and L represent the shortwave and longwave radiative fluxes, respectively. H and LE represent the turbulent fluxes of sensible and latent heat between atmosphere and ocean

served values (e.g. Gordon 1986). The overturning pattern is kept constant throughout the experiments while the overturning strength can be freely altered as desired. Temperature is thus transported as a scalar quantity. The mechanisms taken into account are: overturning, eddy/gyre horizontal transport parametrized as a diffusive process and vertical mixing processes also parametrized as a diffusive process. Sea ice is incorporated in a purely thermodynamic way: when water temperatures drop below the freezing point of saline water, sea ice with a fixed thickness and albedo starts to form. As soon as sea ice is present, the fractional coverage of snow on sea ice is a function of the surface air temperature, similar to snow on land.

Although EBCMs have been proven useful in paleoclimatic modelling (e.g. Hyde et al. 1989; Harvey 1989a), it is important to consider the limitations of such simple climate models when interpreting the results. Besides the obvious limitations of EBCMs (e.g. no explicit dynamics, no vertical resolution in the atmosphere, all physical processes included in parametrized form), one particular limitation of most EBCMs is of special importance when studying the LGM climate: their neglect of zonal asymmetries by using zonal mean quantities. Owing to the location of the major LGM ice sheets, their impact on climate was much larger over the North Atlantic Ocean than over other regions at the same latitudes, as indicated by proxy data (CLIMAP 1981) and by general circulation modelling studies (e.g. Manabe and Broccoli 1985b). The use of a zonally averaged model implies that such a local climate forcing is redistributed instantaneously over an entire latitude zone, which will obviously affect the model response.

The model, which uses realistic land-sea distribution, is tuned to match the present-day climate as closely as possible by adjusting the cloud optical depth. The model successfully reproduces the present-day seasonal cycle of surface air temperatures, radiative fluxes at the top of the atmosphere and at the surface, the turbulent fluxes and the snow cover on land (Bintanja 1995; Bintanja and Oerlemans 1995). There are some discrepancies with regard to the annual range of sea ice in both hemispheres, which is probably due to the neglect of ice dynamics in the sea-ice model. The values of the meridional heat transports seem to agree with the (widely varying) observations, with the atmospheric transport being approximately twice as large as the oceanic transport. While the simulated atmospheric transport peaks at 45°, which is the latitude where the meridional temperature gradient is largest, the oceanic transport peaks at lower latitudes ($\sim 30°$), in accordance with observations. This important aspect is a direct result of the overturning mechanism in our model, where the magnitude of the associated transport is larger than the eddy/gyre oceanic transport.

Model-sensitivity of the current climate

With the current climate sufficiently well simulated, the model can be used to quantify the sensitivity of the present-day climate. The important feedback mechanisms incorporated in this model are the water vapour-temperature feedback and the albedo-temperature feedback. The latter can be subdivided in to the land snow area feedback, the sea-ice area feedback and the snow temperature feedback. By defining a climate sensitivity parameter $\lambda = \Delta T / \Delta Q$, where ΔT is the global mean temperature change resulting from an initial change in radiative forcing at the top of the atmosphere (ΔQ), and using a linear feedback analysis (Harvey 1988b), each of these feedbacks can be easily quantified. As shown by Bintanja and Oerlemans (1995), forcing the model with a 2% decrease in insolation yields reasonable values of the water vapour-temperature feedback ($\lambda^{-1} = -1.05$ W m^{-1} K^{-1}) and albedo-temperature feedback (-0.77 W m^{-1} K^{-1}) (note that a negative value of λ^{-1} indicates a positive feedback). Further, the sea-ice area feedback appears to be about twice as strong as the land snow feedback, while the snow temperature feedback is weak. Bintanja and Oerlemans (1995) showed that these results are in good agreement with estimates from other modelling studies, which indicates that the strength of these feedbacks is incorporated sufficiently well. Also the seasonal and latitudinal distribution of the sensitivity agrees qualitatively with that of GCMs (e.g. Manabe and Stouffer 1980). As these feedbacks will be operative in all subsequent LGM-experiments they will considerably affect the model-response when LGM boundary conditions are applied.

LGM experiments

During the LGM, many potentially important elements of the climate system were different than those of today, such as land-ice cover, atmospheric CO_2-concentration, atmospheric aerosol content, cloud amount, cloud properties, vegetation distribution and oceanic overturning. We have chosen to investigate only the ef-

fect of the first two elements, which are considered to be the most important ones, and, in addition, the effect of oceanic overturning. The other elements have been neglected for the following practical reasons: (1) our radiative transfer parametrization does not allow variations in aerosol content, (2) the use of internal cloud feedbacks is of little significance in EBCMs and (3) the influence of vegetation on surface albedo is not incorporated in such a way that a realistic vegetation-climate feedback is present. It should be realized, though, that the elements not considered here may have a considerable effect on the differences between the LGM and current climate (Manabe and Broccoli 1985b; Harvey 1989a), although according to Broccoli and Manabe (1987), changes in vegetation cover have only a slight impact on the simulation of the LGM climate compared to the impact of land-ice or CO_2.

Manabe and Broccoli (1985b) stated that the latitudinal and seasonal distribution of incident solar radiation at the top of the atmosphere during the LGM was very similar to that of today. It is therefore kept fixed at its current distribution for all experiments described here. The main feature of the LGM was the presence of two major ice sheets in the NH: the Fennoscandian ice sheet in Northern Europe and the Laurentide ice sheet in North America. In addition, nearly all smaller ice caps and glaciers expanded during the LGM. The fractional land-ice cover and the mean surface elevation of the continents during the LGM have been derived from CLIMAP (1976) and CLIMAP (1981). The maximum difference in zonal mean surface elevation over land between the LGM and today due to the presence of ice sheets during the LGM is about 500 m at 67.5 °N (differences in surface elevation affect the longwave cooling of the surface). In contrast to what was previously expected, the LGM elevation distribution of the Antarctic ice sheet differs only slightly from that of the present-day situation, especially in the interior (Denton et al. 1989). However, in the coastal areas of the Antarctic ice sheet there might have been a slight northward expansion and thickening of the land-based ice in connection with a global sea level drop of about 120 m during the LGM. In the present study, the surface elevation of the Antarctic ice sheet in the LGM is assumed to be equal to that in the current climate. The change in fractional land-ice cover between the LGM and present-day is illustrated in Fig. 3. Especially noticeable is the large amount of land-ice in the NH during the LGM compared to that in the current climate, with a maximum coverage of approximately 50% of the total surface area at 62.5 °N.

Ice-core studies have revealed that the atmospheric carbon dioxide concentration during the LGM was about 200 ppmv (Barnola et al. 1987; Neftel et al. 1988), which is about 70 ppm lower than the pre-industrial (interglacial) level (Fig. 4) and 150 ppm lower than the present-day CO_2-content. Therefore, we have used an LGM CO_2-concentration of 200 ppmv, which, according to our radiation scheme, constitutes a direct radiative forcing of -2.9 W m^{-2} at the top of the atmosphere compared to the current CO_2 forcing.

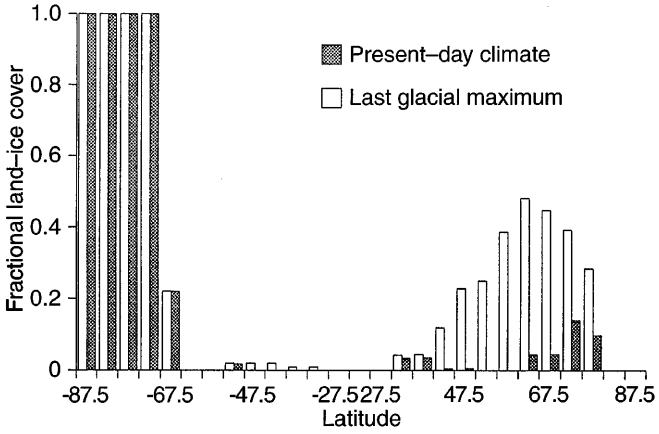

Fig. 3. Fractional land-ice cover in the present-day climate and in the LGM climate (CLIMAP 1976; CLIMAP 1981). The fractional land-ice cover has been scaled with the fraction of land, which means that the fractional coverage of the entire latitude circle is presented here (for instance, a fractional land-ice cover of 0.5 means that 50% of the surface area at that latitude is covered by land ice). Note that the area between 27.5 °N and 27.5 °S is not shown since it does not contain any land ice in both climatic states

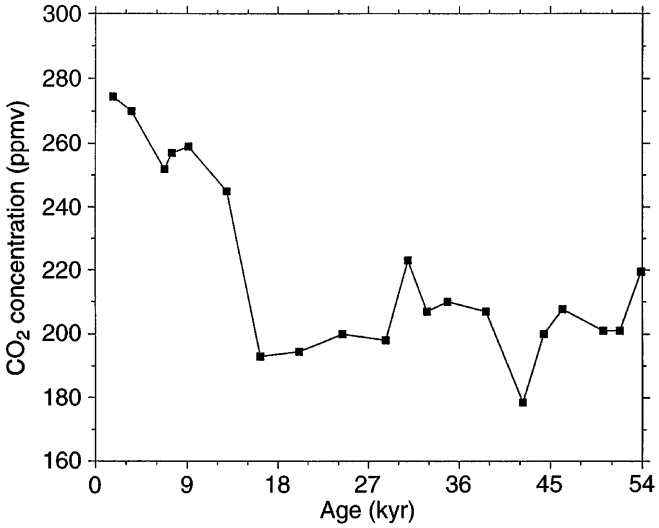

Fig. 4. Variation in atmospheric CO_2-concentration over the last 54000 years obtained from the Vostok ice core, Antarctica (after Barnola et al. 1987)

Finally, it has been suggested that the oceanic overturning rate (C; which is directly proportional to the flow velocities) was significantly reduced during the last ice age. Geochemical evidence obtained from fossil deposits and isotope studies of deep-sea sediments indicates that the production of North Atlantic Deep Water (NADW) was significantly reduced during the LGM, perhaps to one-third to one-half of its present level (Boyle and Keigwin 1982; Corliss 1982; Boyle and Keigwin 1987; Curry et al. 1988). Harvey (1989b) summarized possible reasons for diminished NADW formation during the LGM: (1) a cut-off in the outflow of

Mediterranean Sea water (possibly sea-level regulated), (2) equatorward expansion of sea ice in the North Atlantic Ocean, and (3) reduced evaporation from the North Atlantic Ocean. There are strong indications that the production of intermediate water increased while the NADW flux decreased (e.g. Boyle and Keigwin 1987). Therefore, it may be possible that during the LGM the overturning circulation was shallower than at present while its associated poleward heat transport was of similar magnitude. However, there are several studies that state that reduced poleward heat transport most probably did accompany a reduction in NADW production (e.g. Ruddiman and McIntyre 1981; Broecker et al. 1985; Berger et al. 1987). Broecker and Denton (1989) argued that the conveyor belt circulation was greatly weakened or even absent during glacial periods, and they suggested that this corresponded to one of the possible 'modes' of ocean circulation. Further evidence of the existence of (at least) two modes of ocean circulation with very distinct meridional heat transports was given by Manabe and Stouffer (1988) by using a coupled ocean-atmosphere general circulation model.

The estimates of the temporal changes in the formation of Antarctic Bottom Water are even more uncertain than those in the NH (Crowley and North 1991). However, given all the evidence, it seems not unlikely that, on a global scale, ocean overturning rates were significantly diminished during the last ice age. Also, there are numerous modelling studies that indicate that colder climates are associated with lower overturning rates in a predominantly buoyancy driven ocean (e.g. Manabe and Bryan 1985; Bintanja and Oerlemans 1996). Even though it is unlikely that changes in oceanic overturning were similar in both hemispheres, in the present study it is assumed that they have varied in a similar way. In our simplified ocean formulation a decrease in overturning directly leads to a decrease in poleward heat transport. Since the exact value of the LGM overturning rate is largely unknown at present, three cases will be considered for the reduction in overturning rate in our calculations of the LGM-climate: (1) $C/C_0 = ¼$, (2) $C/C_0 = ½$, and (3) $C/C_0 = ¾$, where C_0 is the present-day overturning rate. In order to simulate the LGM climate the following changes were applied successively, after each of which the model was allowed to re-establish equilibrium:

(1) LGM land-ice fraction
(2) LGM mean surface elevation of continents + (1)
(3) LGM CO_2-concentration = 200 ppmv + (2)
(4) LGM oceanic overturning rate (one of the three cases mentioned above) + (3)

The remaining model parameters are kept at their present-day values. As stated earlier, the response of the model to each of the mentioned perturbations will not only be due to the direct effect of the perturbation itself, but will also be strongly affected by the several operational feedback mechanisms, e.g. the albedo-temperature feedback (snow and sea ice) and the water vapour-temperature feedback.

Results

Global and hemispheric mean model response

The change in global and hemispheric mean surface air temperature for each case is shown in Fig. 5. The decrease in temperature due to the inclusion of LGM land-ice fraction is largest in the NH (2.4 °C) and negligible in the SH. In the NH, the loss of shortwave energy is entirely balanced by the local reduction of upward longwave radiation. Apparently, the ability of the system to transport energy across the equator is limited, a feature consistent with the LGM-simulation of Manabe and Broccoli (1985a), in which an atmospheric GCM coupled to a mixed layer ocean was used. The reduction in atmospheric CO_2 causes a global decrease in temperature, simply because the greenhouse effect is reduced and more longwave radiation can escape to space. In the NH, the CO_2-induced temperature drop is somewhat larger than in the SH. A decrease in oceanic overturning rate further decreases global and hemispheric mean temperatures.

Table 1 shows the difference in surface air temperature between LGM and current climate for each case considered. Increasing the mean surface height of the continent affects temperature only slightly. The lower surface temperature increases the surface albedo only marginally since the additional snow associated with lower temperatures merely covers already highly reflective land ice. For large changes in overturning rate the decrease in temperature is largest, since then the changes in poleward energy transport are largest, allowing greater cooling of the polar seas and hence more sea ice to be formed.

The results indicate that the reduction in oceanic overturning during the LGM contributed significantly to the cooling, especially in the SH. For the case $C/C_0 = ½$ the additional global cooling is 0.9 °C, which is only slightly less than the cooling due to increased

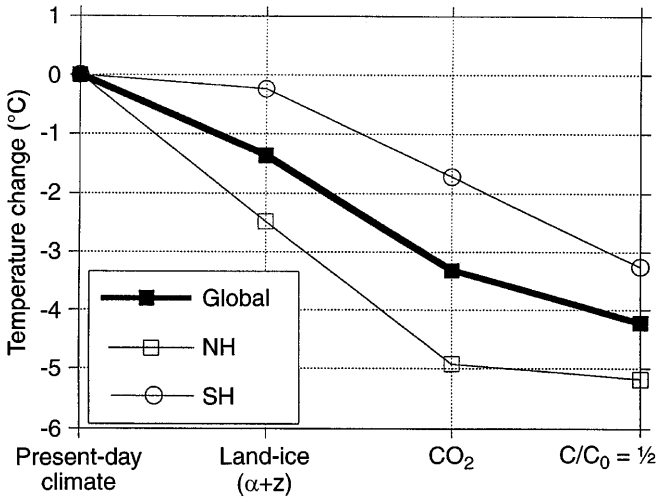

Fig. 5. Difference in annual mean surface air temperature (global and hemispheric mean values) between the LGM and present-day resulting from successive changes in boundary conditions

Table 1. Difference between LGM and present-day globally and hemispherically averaged surface air temperatures (°C) for each variable successively changed. Note that each of the runs with the three cases in oceanic overturning starts with the climatic state for the altered land-ice and CO_2 conditions. Land ice (α) denotes the change in land-ice fractional cover, while land ice (z) denotes the change in mean land surface height

		NH	SH	Global
Land ice (α)		−2.4	−0.3	−1.3
Land ice (z)		−2.5	−0.3	−1.4
CO_2		−4.9	−1.7	−3.3
Oceanic overturning	$C/C_0 = ¾$	−5.0	−2.7	−3.8
	$C/C_0 = ½$	−5.2	−3.3	−4.2
	$C/C_0 = ¼$	−5.4	−3.8	−4.6

land ice. This suggests that variations in ocean overturning may be important for model-based climatic reconstructions of the LGM.

The SH is very sensitive to a change in oceanic overturning since there the interaction with the albedo-temperature feedback (sea-ice area) is strongest. Apparently, the decrease in poleward oceanic transport sufficiently reduces ocean temperatures near the SH sea-ice border which allows strong sea-ice expansion. This clearly illustrates the importance of the interaction between two or more feedback mechanisms, and the fact that the strength of the individual feedback mechanisms must be represented well.

In each of the scenarios, the *total* (i.e. cumulative) SH temperature differences are smaller than those in the NH. The simulated decrease of 4.2 °C (3.3 °C without changes in oceanic overturning) in the global mean surface air temperature compares reasonably well with the estimates of Hansen et al. (1984) and Manabe and Broccoli (1985b), whose calculations showed that LGM temperatures were 3.6 °C lower than today (both studies did not incorporate variations in oceanic circulation). Most of the other studies referred to (of which some include other cooling mechanisms) predicted global mean LGM surface air temperatures that are 3.5–4.0 °C lower than present.

Latitudinally varying response

The meridional distribution of annual mean change in surface air temperature and sea-surface temperature (SST) is presented in Fig. 6. Obviously, the inclusion of LGM land-ice distribution affects mainly the NH, and leads to a maximum decrease in air temperature of 7.5 °C at the North Pole. The SST change is maximum at 57.5° N, where it amounts to −3.5 °C. The SST at higher latitudes cannot change much due to the presence of sea-ice in both the current state as well as in the LGM climate with SST values close to the freezing point. A significant contributor to the colder LGM climate in *both* hemispheres is the reduction of CO_2. The LGM air temperatures are more than 12 °C lower in the north polar region and about 3 °C lower in the

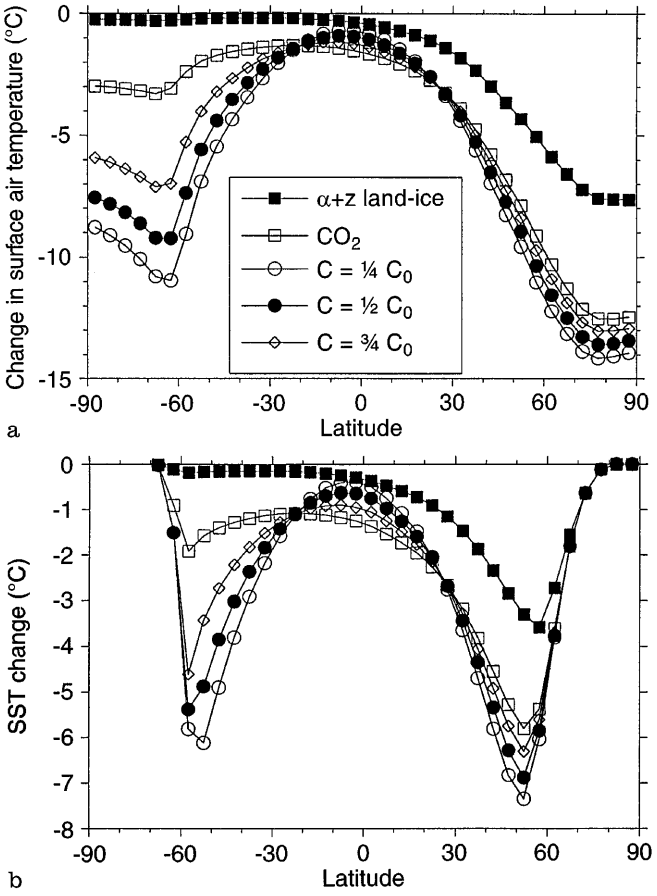

Fig. 6a. Meridional distribution of the zonal and annual mean differences between the LGM and present-day surface air temperatures and **b** sea-surface temperatures for the various cases

south polar region due to both reduced LGM CO_2-concentrations and increased amount of land ice. These results are in good qualitative agreement with those of Broccoli and Manabe (1987).

The inclusion of a reduced oceanic overturning rate significantly reduces LGM surface air temperatures and SST in the SH, whereas in the NH the temperature changes due to overturning variations are small. In the SH, the change in overturning rate seems to be the largest contributor to the differences between the LGM and the current climate, especially for large reductions in C. There, the increased cooling due to a decreased overturning ($C/C_0 = ¼$) amounts to 7 °C and 4 °C in case of surface air temperature and SST, respectively. A decrease in overturning rate reduces the amount of energy transported poleward by the oceans. As a result, temperatures in the tropics increase compared to the cases without alterations in overturning rate.

Smaller overturning rates directly result in a smaller poleward heat transport in the oceans. On the other hand, the increasing meridional temperature gradient in the atmosphere leads to a larger atmospheric poleward transport of energy. Figure 7 depicts the difference in meridional heat transport between the LGM ($C/C_0 = ½$) and the present-day climate. In the LGM

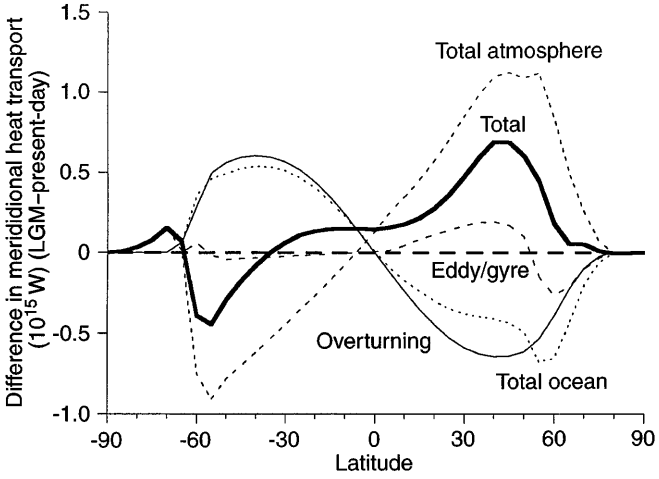

Fig. 7. Meridional distribution of the difference in zonal and annual mean meridional heat transport terms between the LGM ($C/C_0 = ½$) and the present-day climate. A positive difference indicates a larger northward transport during the LGM

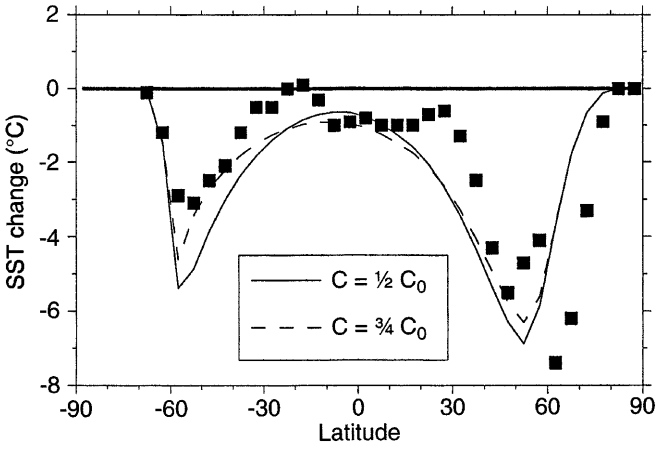

Fig. 8. Meridional distribution of the difference in zonal and annual mean SST between the LGM and current climate. The *lines* are model results for two LGM cases ($C/C_0 = ½$ and $C/C_0 = ¾$), whereas *squares* represent CLIMAP data

climate, total ocean transport is about 40–50% lower and total atmospheric transport about 30–35% higher than in the current climate. However, absolute changes in atmospheric transport dominate over the changes in ocean transport, especially in the NH where, at 45 °N, the LGM total poleward heat transport is about 0.7×10^{15} W larger than today. This might explain the greater sensitivity of the SH for variations in ocean overturning, since there the decrease in poleward oceanic transport is more in balance with the increase in atmospheric transport, resulting in smaller changes in total transport when compared to the NH. In other words, the atmosphere-ocean system in the SH is less capable of restoring energy perturbations at higher latitudes, which acts to increase the strength of the albedo-temperature feedback.

Obviously, a decrease in ocean overturning causes equatorial temperatures to rise and polar temperatures to decrease (Fig. 6). The CO_2-induced decrease in LGM equatorial temperatures is partially offset by this effect. Over Antarctica, LGM surface air temperatures are 7.5–9.0 °C lower than today in the $C/C_0 = ½$ case, which is in good agreement with the estimate of Jouzel et al. (1987). From oxygen-isotope analyses of the Vostok ice-cores they estimated that Antarctic LGM-temperatures were 8–10 °C lower than the at present. Without reduced ocean overturning, our model predicts temperature differences of only about 3 °C over the Antarctic continent, which again demonstrates the potential importance of variable ocean circulation for climate change studies.

Comparison with CLIMAP SST

The reconstructed LGM SST-distribution provided by CLIMAP is compared with the model-derived values (for the cases $C/C_0 = ½$ and $C/C_0 = ¾$) and is shown in Fig. 8 as deviation from the present-day SST-distribution. The model seems to capture all major features of the LGM temperature distribution except for the small-scale structures. The maximum SST differences in the NH are larger than in the SH, both in the model and in the data. However, maximum simulated SST-differences seem to be too large in the SH and too small in the NH, which might be attributed to, for instance, the fact that, in reality, the changes in NH and SH oceanic overturning rates were not equal (which seems very plausible). The small temperature differences in the equatorial region as suggested by the CLIMAP-data seem to be captured by the model, although the LGM subtropical temperatures are underestimated by a few degrees. The latter seems to be a general feature of most of the model studies mentioned.

In order to evaluate the quantitative agreement of the results, Table 2 gives some statistics of the differences between model-derived SST and CLIMAP SST for various oceanic overturning cases. Decreasing the overturning rate acts to enhance the difference between model and CLIMAP SST due to the cooling caused by the albedo-temperature feedback. However, the mean difference has little meaning as positive and negative deviations can cancel each other out. According to the correlation coefficient between CLIMAP and model-generated SST, the best agreement is obtained in case of $C/C_0 = ¾$. The same conclusion might be drawn when considering global mean squared differences, which are smallest for $C/C_0 = ¾$. For larger reductions in overturning rate the squared differences tend to increase drastically. A similar feature is apparent when the true global mean value is calculated, in which the meridional variation in ocean surface area is taken into account. In this way, the global mean squared differences obviously become smaller because of the dominant influence of the larger surface area in the equatorial region where the squared differences are relatively small. Considering regional variations in the squared differences between simulated and CLI-

Table 2. Statistics of the difference between annual mean model-generated SST and CLIMAP SST for various oceanic overturning rates. An asterisk indicates that the mean squared differences were obtained by weighting with the fractional ocean area

	$C/C_0=1$	$C/C_0=¾$	$C/C_0=½$	$C/C_0=¼$
Global mean difference	−0.01	−0.28	−0.45	−0.62
Correlation coefficient	0.67	0.71	0.69	0.67
Global mean squared difference	2.12	2.11	2.59	3.38
Global mean squared difference*	1.22	1.15	1.65	2.52
Squared difference (70 °S–30 °S)*	0.75	0.58	1.98	4.26
Squared difference (30 °S–30 °N)*	0.92	0.76	0.70	0.76
Squared difference (30 °N–90 °N)*	2.94	3.30	3.95	4.87

MAP SST, it appears that the SH extratropical and the equatorial regions benefit most from a reduction in oceanic overturning. There, the squared SST differences are smallest for $C/C_0=¾$ and $C/C_0=½$, respectively. In fact, the agreement in the tropics seems to increase for any reduction in ocean overturning, which implies that without variations in ocean overturning the simulated LGM equatorial temperatures are far too low compared to CLIMAP SST. The agreement in the NH extratropical region becomes less with inclusion of reduced overturning rates. Although the differences in statistical values between some of the cases are not overwhelming, this analysis nevertheless indicates that the best agreement between our model-derived SST and CLIMAP SST is obtained by assuming that, in the present model outline, LGM oceanic overturning rates were about 25% smaller than today.

These results suggest that the apparent stability of (sub-)tropical SST might have been linked to variations in oceanic overturning rate during the last 18 ky. The CO_2-induced cooling in the tropics is partially offset by warming due to a reduced oceanic poleward heat transport, which results in a fairly good agreement between model and CLIMAP-data in the equatorial region. In this respect, we must note that Rind and Peteet (1985) stated that LGM tropical and subtropical land temperatures were probably 3–4 °C cooler than today based on snowline and pollen data; this obviously disagrees with our findings, although one should again realize that a number of 'potential cooling' mechanisms were not included in the present study, as discussed in the previous section. The prevailing equatorial temperatures during the LGM are still a matter of some controversy (Broecker and Denton 1989; Anderson and Webb 1994). However, Sun and Lindzen (1993) showed that altitude-dependent temperature differences between the LGM and today are not necessarily inconsistent. Recently, matters became even more complicated when Guilderson et al. (1994) reported LGM SST values 5 °C colder than today as recorded in Barbados corals. Until final conclusions about this matter are made, we will assume that the SST values as given by CLIMAP (1976; 1981) represent the correct LGM temperatures.

Although the simplicity of the applied changes in ocean overturning may be critized (in particular, it is very unlikely that the changes in overturning were the same in both hemispheres), these results demonstrate the potential impact of variations in ocean overturning rate during climatic changes. It is possible that better agreement between simulated and CLIMAP-reconstructed SST, especially in the subtropical regions, can be obtained if a coupled atmosphere-ocean general circulation model is used to study the LGM-climate. Such an approach would be the next logical step in exploring the role of the oceans in glacial-interglacial climate variations.

Seasonally varying response

The latitudinal and seasonal distribution of the differences in surface air temperature between the LGM and current climate is shown in Fig. 9a. For reasons similar to those given by Manabe and Stouffer (1980), the temperature differences between LGM and today are largest in winter. In the north polar region in early winter, LGM temperatures are 15 °C lower than today. However, the difference in annual temperature range in the north polar region between the LGM and current climate is smaller than for example the $2\times CO_2$-case. This is due to the fact that during the LGM a continuous (i.e. year-round) cooling occurs due to the presence of the highly reflective ice sheets. This cooling will be largest in summer when solar insolation is at its maximum. In contrast, the sea-ice area feedback causes maximum temperature differences in winter (e.g. Manabe and Stouffer 1980; Bintanja and Oerlemans 1995). The simultaneous impact of these two effects allow the average annual temperature range in the north polar region (70°–90 °N) to increase by only 2 °C. Also the temperature differences between 0° and 60° seem to be almost seasonally invariant. In the SH, the only effect is an increase in sea ice, causing the LGM annual temperature range to be 4–6 °C larger than today.

Figure 9b shows the same as in Fig. 9a but with the overturning rate kept at its present-day value. It can be inferred that in the SH around 60° S, at the marginal sea-ice border, the cooling due to reduced overturning is maximum in winter. As a result, the annual range in atmospheric temperature at 60° S increases by 4.5 °C compared to the case without changes in overturning. In the NH, decreased overturning causes a slight increase in annual temperature range of about 0.7 °C (at 60 °N). These results again suggest that the sea-ice area

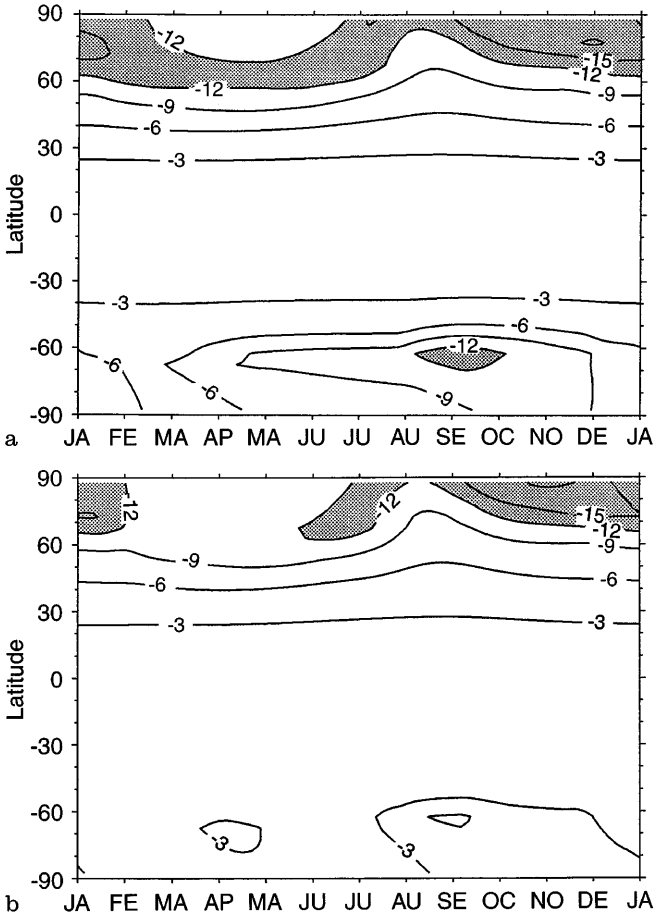

Fig. 9a. Latitude-time distribution of the difference in zonal mean surface air temperature (°C) between the LGM climate with reduced overturning ($C/C_0 = ½$) and the present-day climate and **b** the LGM climate with present-day overturning ($C/C_0 = 1$) and the present-day climate. *Grey* areas indicate LGM temperatures of 12 °C or more lower than today

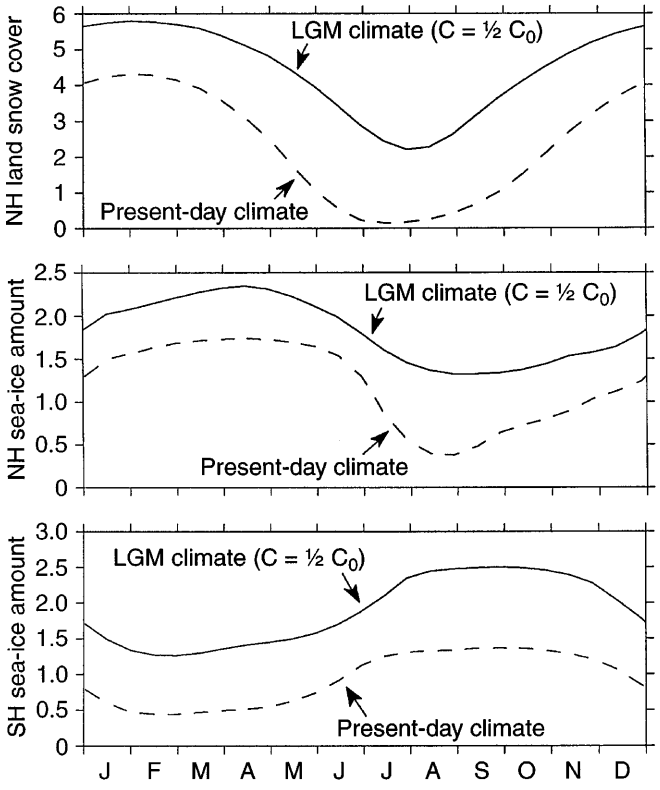

Fig. 10. Simulated seasonal cycle of zonal mean NH land snow cover, NH sea-ice cover and SH sea-ice cover (10^{13} m^2) for the present-day climate and the LGM climate. Note that each diagram has different vertical scales

feedback, which causes maximum air temperature changes in winter, is largely responsible for the large sensitivity of the SH for reductions in ocean overturning.

Sea ice, snow and albedo

The seasonal variation of LGM and present-day amount of sea-ice and of snow cover is presented in Figure 10. The increase in sea ice for the LGM climate is largest in the NH summer and in the SH winter. In the SH winter, the amount of LGM sea ice is approximately twice as much as in the present climate, which is in agreement with the findings of Cooke and Hays (1982). In the NH, the absolute increase in sea ice is smaller. Further, its annual range is smaller during the LGM, which can be attributed mainly to the cold NH summers. The equatorward boundary of the sea-ice pack shifts from 80° (present-day) to 65° (LGM) and from 65° to 53° in NH summer and winter, respectively. Due to the absence of continents in the SH marginal sea-ice region, the equatorward shift of the sea-ice border in the SH is much smaller: from 62° (present-day) to 57° (LGM) and from 68° to 62° in SH summer and winter, respectively.

The NH snow cover increases by a maximum of 3×10^{13} m^2 in spring and early summer in the LGM climate. In contrast to what might be expected, the maximum change in snow cover occurs when the change in sea ice is smallest. This is probably due to the fact that the large ice masses on the NH continents cause spring and summer cooling especially over land.

The SH land snow cover during the LGM was only slightly larger than for the present-day climate, with virtually no seasonal variation. Apparently, LGM temperatures in the SH were still high enough to prevent the occurrence of significant snow cover on the land masses outside Antarctica, even in winter. The differences in annual mean amounts of sea-ice and land snow cover between the LGM and current climate are given in Table 3.

Table 3. Annual mean amounts of sea-ice and land snow cover for the LGM and the present-day climate (10^{13} m^2)

	Sea ice		Land snow cover	
	NH	SH	NH	SH
Present-day climate	1.20	0.92	2.37	1.73
LGM climate ($C/C_0 = ½$)	1.82	1.88	4.46	1.78

Table 4. Difference in global and annual mean planetary albedo and surface albedo between the LGM and present-day climate for both polar regions. The values for the LGM climate are given in brackets

	North polar region		South polar region	
	70°–90°	60°–90°	70°–90°	60°–90°
Surface albedo	0.25 (0.78)	0.32 (0.70)	0.00 (0.82)	0.17 (0.74)
Planetary albedo	0.17 (0.79)	0.21 (0.72)	0.02 (0.83)	0.12 (0.76)

The impact of larger amounts of sea ice and snow during the LGM on the annual mean albedo of the polar regions is presented in Table 4. Obviously, the albedo differences are largest in the NH, which is due mainly to the increase in land ice and snow on land. Especially over the south polar region the difference between the two cases (70°–90° and 60°–90°) is considerable since the largest differences in albedo obviously occur when the marginal sea-ice zone is included.

Summary and conclusions

In order to obtain insight in the causes of glacial-interglacial climatic differences, the climate of the Last Glacial Maximum (LGM) (18 ky BP) is simulated with an energy balance climate model coupled to a simple advection-diffusion ocean model. The following LGM boundary conditions are applied: enhanced coverage of land ice, a decrease in atmospheric CO_2-content and a decrease in oceanic overturning. The high surface albedo of the large land-ice masses during the LGM accounts for a maximum annual mean temperature decrease of 7.5 °C in the NH and almost no change in the SH as compared to the temperature distribution in the present-day climate. The reduced CO_2-concentration further reduces temperatures in both hemispheres. A reduction of 50% in oceanic overturning causes a significant extra cooling in the SH, practically no additional cooling in the NH and a reduction in the cooling in the equatorial region. These effects are more pronounced for larger reductions in ocean overturning. The positive albedo-temperature feedback (especially through sea-ice variations) significantly contributes to the differences between the LGM and present-day climate.

The simulated and CLIMAP sea-surface temperatures compare reasonably well, even without changes in oceanic overturning rate. The agreement slightly improves if a reduction in oceanic overturning is applied, especially in the equatorial region where, according to CLIMAP data, the difference in sea-surface temperatures between LGM and today is small, but also over Antarctica in case of the surface air temperature. Overall, the best agreement was found for a reduction in oceanic overturning of 25%. The reduced heat loss from the tropical oceans due to reduced poleward heat transport resulting from lower overturning rates might be responsible for the relatively slight variations in equatorial surface temperatures during the last 18000 years. However, due to the simplicity of our model only the large-scale effects of this mechanism could be qualitatively investigated here. Coupled atmosphere-ocean models of higher complexity will be needed to assess the impact of variations in ocean circulation on past climates in more detail.

Acknowledgements. Jan de Wolde is recognized for his valuable comments on an earlier version of the manuscript. Financial support was provided by the Netherlands Antarctic Research Programme (GOA). This work was sponsored by the National Computing Facilities Foundation (NCF) for the use of supercomputing facilities, with financial support from the Netherlands Organization for Scientific Research (NWO).

References

Anderson DM, Webb RS (1994) Ice-age tropics revisited. Nature 367:23–24

Barnola JM, Raynoud D, Korotkevich YS, Lorius C (1987) Vostok ice core provides 160000-year record of atmospheric CO_2. Nature 329:408–414

Berger WH, Burke S, Vincent E (1987) Glacial-Holocene transition: climatic pulsations and sporadic shutdown of NADW production. In: Berger WH, Labeyrie LD (eds) Abrupt climate change. Reidel, Dordrecht, pp 279–297

Bintanja R (1995) The Antarctic ice sheet and climate. Ph D Thesis, Utrecht University, pp 1–232

Bintanja R (1996) The parametrization of shortwave and longwave radiative fluxes for use in zonally averaged climate models. J Clim 9:439–454

Bintanja R, Oerlemans J (1995) The influence of the albedo-temperature feedback on climate sensitivity. Ann Glaciol 21:353–360

Bintanja R, Oerlemans J (1996) Variations in ocean overturning and climate sensitivity: application of a zonal average climate model. Clim Dyn (submitted)

Boyle EA, Keigwin L (1982) Deep circulation of the North Atlantic over the past 200000 years: geochemical evidence. Science 218:784–787

Boyle EA, Keigwin L (1987) North Atlantic thermohaline circulation during the past 20000 years linked to high-latitude surface temperature. Nature 330:35–40

Broccoli AJ, Manabe S (1987) The influence of continental ice, atmospheric CO_2 and land albedo on the climate of the last glacial maximum. Clim Dyn 1:87–99

Broecker WS, Denton GH (1989) The role of ocean-atmosphere reorganizations in glacial cycles. Geochim Cosmochim Acta 53:2465–2501

Broecker WS, Peteet DM, Rind D (1985) Does the ocean-atmosphere system have more than one stable mode of operation? Nature 315:21–26

CLIMAP Project Members (1976) The surface of the ice-age earth. Science 191:1131–1137

CLIMAP Project Members (1981) Seasonal reconstructions of the earth's surface at the last glacial maximum. Geol Soc Am Map Chart Ser, MC-36

Cooke DW, Hays JD (1982) Estimates of Antarctic Ocean seasonal sea-ice cover during glacial intervals. In: Craddock C et al. (eds) Antarctic geoscience. University of Wisconsin Press, Madison, pp 1017–1025

Corliss BH (1982) Linkage of North Atlantic and Southern Ocean deep-water circulation during glacial intervals. Nature 298:458–460

Crowley TJ, North GR (1991) Paleoclimatology. Oxford University Press, New York

Curry WB, Duplessy J-C, Labeyrie LD, Shackleton NJ (1988) Changes in the distribution of $\delta^{13}C$ of deep water ΣCO_2 between the last glaciation and the Holocene. Paleoceanography 3:317–341

Denton GH, Bockheim JG, Wilson SC, Stuiver M (1989) Late Wisconsin and early Holocene glacial history, inner Ross Embayment, Antarctica. Quat Res 31:151–182

Gates WL (1976) The numerical simulation of ice-age climate with a global general circulation model. J Atmos Sci 33:1844–1873

Gordon AL (1986) Interocean exchange of thermocline water. J Geophys Res 91:5037–5046

Guilderson TP, Fairbanks RG, Rubenstone JL (1994) Tropical temperature variations since 20000 years ago: modulating interhemispheric climate change. Science 263:663–665

Hansen JE, Lacis A, Rind D, Russell G, Stone P, Fung I, Ruedy R, Lerner J (1984) Climate sensitivity: analysis of feedback mechanisms. In: Hansen JE, Takahashi T (eds) Climate processes and climate sensitivity. Geophys Monogr Ser 29; American Geophysical Union, Washington DC, pp 130–163

Harvey LDD (1988a) A semianalytic energy balance climate model with explicit sea ice and snow physics. J Clim 1:1065–1085

Harvey LDD (1988b) On the role of high latitude ice, snow, and vegetation feedbacks in the climate response to external forcing changes. Clim Change 13:191–224

Harvey LDD (1989a) An energy balance climate model study of radiative forcing and temperature response at 18 ka. J Geophys Res 94:12873–12844

Harvey LDD (1989b) Milankovitch forcing, vegetation feedback, and North Atlantic deep-water formation. J Clim 2:800–815

Hoffert MI, Callegari AJ, Hsieh C-T (1980) The role of deep sea heat storage in the secular response to climate forcing. J Geophys Res 85:6667–6679

Hyde WT, Crowley TJ, Kim KY, North GR (1989) Comparison of GCM and energy balance simulations of seasonal temperature changes over the past 18000 years. J Clim 2:864–887

Jouzel J, Lorius C, Petit JR, Genthon C, Barkov NI, Kotlyakov VM, Petrov VM (1987) Vostok ice core: a continuous isotope temperature record over the last climatic cycle (160000 years). Nature 329:403–408

Kutzbach JE, Guetter PJ (1986) The influence of changing orbital parameters and surface boundary conditions on climate simulations for the past 18000 years. J Atmos Sci 43:1726–1759

Manabe S, Stouffer RJ (1980) Sensitivity of a global climate model to an increase of CO_2 concentration in the atmosphere. J Geophys Res 85:5529–5554

Manabe S, Stouffer RJ (1988) Two stable equilibria of a coupled ocean-atmosphere model. J Clim 1:841–866

Manabe S, Bryan K (1985) CO_2-induced change in a coupled ocean-atmosphere model and its paleoclimatic implications. J Geophys Res 90:11689–11707

Manabe S, Broccoli AJ (1985a) The influence of continental ice sheets on the climate of the ice age. J Geophys Res 90:2167–2190

Manabe S, Broccoli AJ (1985b) A comparison of climate model sensitivity with data from the last glacial maximum. J Atmos Sci 42:2643–2651

Neftel A, Oescher H, Schaffelbach T, Stauffer B (1988) CO_2 record in the Byrd ice core 50000–5000 years BP. Nature 331:609–611

Oerlemans J (1980) Model experiments on the 100000-year glacial cycle. Nature 287:430–432

Oglesby RJ (1990) Sensitivity of glaciation to initial snow cover, CO_2, snow albedo, and oceanic roughness in the NCAR CCM. Clim Dyn 4:219–235

Peltier WR, Marshall S (1995) Coupled energy-balance/ice-sheet model simulations of the glacial cycle: a possible connection between terminations and terrigenous dust. J Geophys Res 100:14269–14289

Pollard D (1982) An investigation of the astronomical theory of the ice ages using a simple climate-ice sheet model. Nature 296:334–338

Rind D (1987) Components of the ice age circulation. J Geophys Res 92:4241–4281

Rind D, Peteet D (1985) Terrestrial conditions at the last glacial maximum and CLIMAP sea-surface temperature estimates: are they consistent? Quat Res 24:1–22

Rind D, Kukla G, Peteet D (1989) Can Milankovitch orbital variations initiate the growth of ice sheets in a general circulation model? J Geophys Res 94:12851–12871

Robock A (1980) The seasonal cycle of snow cover, sea ice and surface albedo. Mon Weather Rev 108:267–285

Ruddiman WF, McIntyre A (1981) Oceanic mechanisms for amplification of the 23000–year ice-volume cycle. Science 212:617–627

Sun D-Z, Lindzen RS (1993) Water vapor feedback and the ice age snowline record. Ann Geophys 11:204–215

Watts RG, Morantine M (1990) Rapid climatic change and the deep ocean. Clim Change 16:83–97